*Earth and Planetary Science Letters*, 96 (1990) 367–383
Elsevier Science Publishers B.V., Amsterdam – Printed in The Netherlands



[CH]

# Gravity anomalies, the deep structure, and dynamic processes beneath the Tien Shan

E.V. Burov [1], M.G. Kogan [1], Hélène Lyon-Caen [2] and Peter Molnar [3,4]

[1] *Institute of Physics of the Earth, Academy of Sciences of the U.S.S.R., B. Gruzinskaya 10, Moscow D-242 (U.S.S.R.)*
[2] *Laboratoire de Sismologie, Institut de Physique du Globe, 4, place Jussieu, 75252 Paris Cedex 05 (France)*
[3] *Department of Earth Sciences, Oxford University, Parks Road, Oxford, OX1 3PR (U.K.)*
[4] *Department of Earth Atmospheric, and Planetary Sciences, Massachusetts Institute of Technology, Cambridge, MA 02139 (U.S.A.)*

Received June 30, 1989; revised version accepted October 19, 1989

Bouguer gravity anomalies over the Tien Shan and Pamir are large and negative, and therefore consistent with crustal thickening beneath both mountain ranges. Gravity anomalies over the western Tien Shan are within about 10 mgal of those expected for local Airy isostatic equilibrium, but those over the eastern Tien Shan are up to 50 mgal too large and negative. Thus they require static or dynamic support of an uncompensated mass deficit. These gravity anomalies cannot be matched using regional compensation of the weight of the range on a continuous elastic plate. A simple model of two separate elastic plates extending north and south from the axis of the Tien Shan can allow an adequate fit of observed and calculated anomalies. The flexural rigidity of the northern plate must be quite small ($D < 10^{23}$ N m, corresponding to an equivalent effective elastic thickness $T_E < 25$ km), but that of the southern plate must be larger ($D \approx 10^{24}$ N m, $T_E \approx 50$–60 km). The data for the eastern Tien Shan cannot be fit without a force per unit length of roughly $1–4 \times 10^{12}$ N, or by a bending moment, applied to the end of the southern plate. Thus either a deep mass per unit length of about $1–4 \times 10^{11}$ kg/m must underlie the eastern part of the range, or dynamic (deviatoric tensional) normal stresses of up to about 5 MPa, due to flow in the asthenosphere, must pull the Tien Shan down. Probably a combination of them, resulting from the formation and sinking of a thickened lithospheric root, causes the deflection of the Moho and the deviations from local isostatic equilibrium.

## 1. Introduction

Most mountain building occurs when and where two plates of lithosphere converge with one another, whether the plate boundary be between an oceanic plate and a continental margin, as along the Andes, or between two continents. Many belts evolve from the first to second, when a continent carried by a subducting plate of oceanic lithosphere eventually collides with the overriding continent. Most such mountain building occurs near to where the two continents are sutured together; the Himalaya, the Alps, the Appalachian–Caledonian chain, and the Urals are noted examples of this phenomenon.

The Tien Shan is probably the Earth's most spectacular active example of a mountain range where these processes neither are happening, nor have happened in Cenozoic time, but where, nevertheless, active convergence of the lithosphere on the two flanks of the range is rapid. The range is laced with active thrust and strike-slip faults, and the seismicity of the Tien Shan is particularly high, with four events with magnitudes exceeding 8 in this century, and a comparable number in the last century [1–5]. As discussed below, a couple of arguments suggest an average rate of convergence across the chain of 5–20 mm/a, making the Tien Shan the most active intracontinental mountain range in the world. As such it probably is the best active analogue for the style and distribution of deformation that created the Rocky Mountains of Colorado, Utah, and Wyoming, in the western United States in Late Cretaceous and Early Tertiary time [6–8]. Yet, the region is remote and much less thoroughly studied than the major ancient ranges of the Earth, and what is known does not, at present, offer strong constraints on the physical processes that occur in the Tien Shan or the reasons for why that area is the locus of active

0012-821X/90/$03.50 

mountain building. One of the important questions that must be addressed in order to answer such questions is: How does the deep structure of the Tien Shan differ from that of the region surrounding it?

Conservation of mass in regions where crustal shortening and crustal thickening form mountain belts requires convergence, if not also thickening, of the mantle lithosphere beneath the range or near to it [9,10]. The mantle lithosphere, which underlay the crust that later was thickened, either must have shortened horizontally and thickened as well or must have detached from the overlying crust to plunge into the asthenosphere. In the latter case, one slab of continental lithosphere might be underthrust beneath another, as occurs in oceanic regions, and as seems to have occurred in the Alps or the Himalaya. If continental crust can be detached from its mantle lithosphere, then the cold, negatively buoyant, mantle lithosphere might plunge into the asthenosphere, drawing the trailing part of intact lithosphere with it. There are suggestions, from gravity anomalies and from travel times of seismic waves, that this process occurs beneath the Alps [11], beneath the Himalaya [12,13] and beneath the Transverse Ranges of California [14,15].

In intracontinental mountain belts, where crustal shortening is not localized on one major thrust fault but is distributed over a wide zone, distributed thickening of mantle lithosphere beneath the belt of shortened and thickened crust should, temporarily, form a lithospheric root beneath chain. Advection of cold, and hence dense, material downward into the asthenosphere will create lateral temperature gradients in the mantle, which could induce convective downwelling beneath the mountain belt. Such convective flow, in turn, would affect the thermal structure of the belt and might enhance the crustal shortening [9,10]. In any case, plausible scenarios for the mantle dynamics beneath mountain belts are sufficiently numerous and different, that the existence of such lithospheric roots cannot be established on theoretical grounds alone. The possibility that such a process is occurring beneath the Tien Shan was a motivation for the present study, and here we present a preliminary study of gravity anomalies across the Tien Shan, as a constraint on the structure and mantle dynamics beneath the chain.

## 2. The Tien Shan

Although the rocks of the Tien Shan were intensely deformed in Late Paleozoic time [16–20], when the Tarim block of Precambrian rock apparently collided with Siberia [21–23], relief associated with that belt had been eroded by the Cenozoic Era. Then, apparently beginning in the Oligocene Epoch [24], or perhaps later, in the Miocene Epoch [23], the region was rejuvenated by intracontinental tectonic activity. Abundant evidence for thrust faulting throughout the present Tien Shan [16,17,23,25–29] indicates that the present range was built by crustal shortening and crustal thickening.

Fault plane solutions of earthquakes demonstrate continued thrust faulting and north-northwest–south-southeast crustal shortening roughly perpendicular to the overall trend of the range [8,29–33], and seismic refraction profiles indicate a thicker crust than normal [34–36]. From rough estimates of variations in crustal thickness across the Tien Shan, Ulomov [34] inferred at least 100 km of Cenozoic crustal shortening, and Molnar and Tapponnier [37] considered 200–300 km possible, if an upper limit. Finally, the deformation and seismic moments associated with major earthquakes in the 20th century suggest a rate of convergence between the Tarim block and the Siberian shield of between 5 and 20 mm/a [4]. Thus, the rate and the amount of shortening in the Tien Shan are probably the largest of any active intracontinental mountain chain in the world, and both of these quantities are comparable with those for the Himalaya. Correspondingly, the Tien Shan is a major active mountain chain where the deep structure might show systematic lateral variations related to Cenozoic crustal shortening.

To a first approximation, the Tien Shan is a linear chain with a roughly constant width of 300–500 km and constant mean elevation of about 2000 m (Fig. 1). At its west end, it diverges, and the two branches surround the relatively small Fergana basin (40–41° N, 70–72° E), which is bounded on three sides by high mountains. The southern branch, or South Tien Shan, lies adjacent to the Pamir, whose geologic history is quite different from that of the Tien Shan. At the east end of the Tien Shan, the belt diffuses into a series of roughly parallel ranges that bound east–west

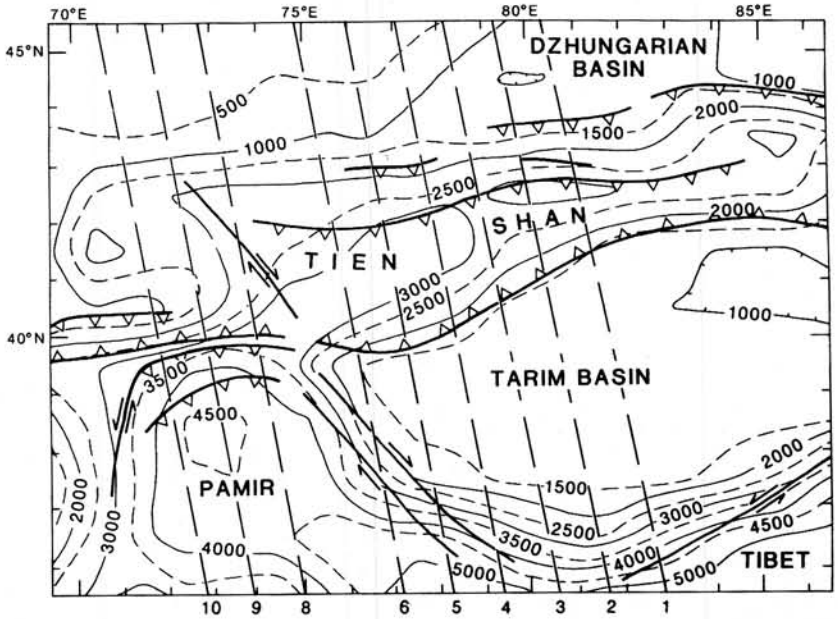


Fig. 1. Contour map of 1° × 1° mean elevations of the Tien Shan, Pamir, and Tarim Basin, showing portions of the profiles of the gravity anomalies across these areas that we analyzed. Major, active thrust faults are shown as dark lines with teeth on the downdip sides.

trending basins; slip on reverse faults has allowed the ranges to be thrust over the basins and the weight of the ranges apparently has deepened the floors of these basins, which are only a few tens of kilometers wide [33]. Let us confine our attention to regions east of the Pamir and west of the area where the Tien Shan consists of separate high ranges and narrow deep basins.

Along the southern margin of the Tien Shan, Paleozoic sedimentary rock is folded, and thrust faults dip north beneath the chain [16,17,33]. Terman et al. [38] showed a deep basin, filled with several kilometers of Cenozoic sediment, along the southern margin of the range. Large variations, however, in their indicated depths of the basement along the southern margin of the basin suggest that the flexure of the basin floor may vary along the chain. Similar basins along the northern margin of the range seem to be present, but the eastern (Chinese) and western (Soviet) parts appear to be quite different. The relatively deep Dzungarian Basin north of the Tien Shan in China appears to be similar to the basins along the southern margin of the chain. Presumably, just as the floor of the Tarim Basin is underthrust northward beneath the Tien Shan, the floor of the Dzungarian basin is underthrust southward beneath the range. In the Soviet Union, north of Tien Shan, the evidence for a flanking basin, like the Dzungarian Basin, is less clear. Although the floor of the Kazakh platform has probably been underthrust southward beneath the chain, the amount of underthrusting, or the recency of its occurrence, seems to be less than that of the Dzungarian Basin or of the Tarim Basin on the south side. Hence, whereas the easternmost part of the range seems roughly symmetrical with underthrusting of both margins beneath it, the western part seems much more asymmetrical, with apparently only minor recent underthrusting of the northern side. In any case, these variations along the chain clearly are small compared with those across it, and a two-dimensional analysis is justified.

## 3. Profiles of gravity anomalies

The data consist of average gravity anomalies, including terrain corrections, and corresponding average elevations over regions with dimensions of 1° × 1°. We constructed profiles approximately perpendicular to the range by projecting 1° × 1° average Bouguer anomalies from regions within 1°

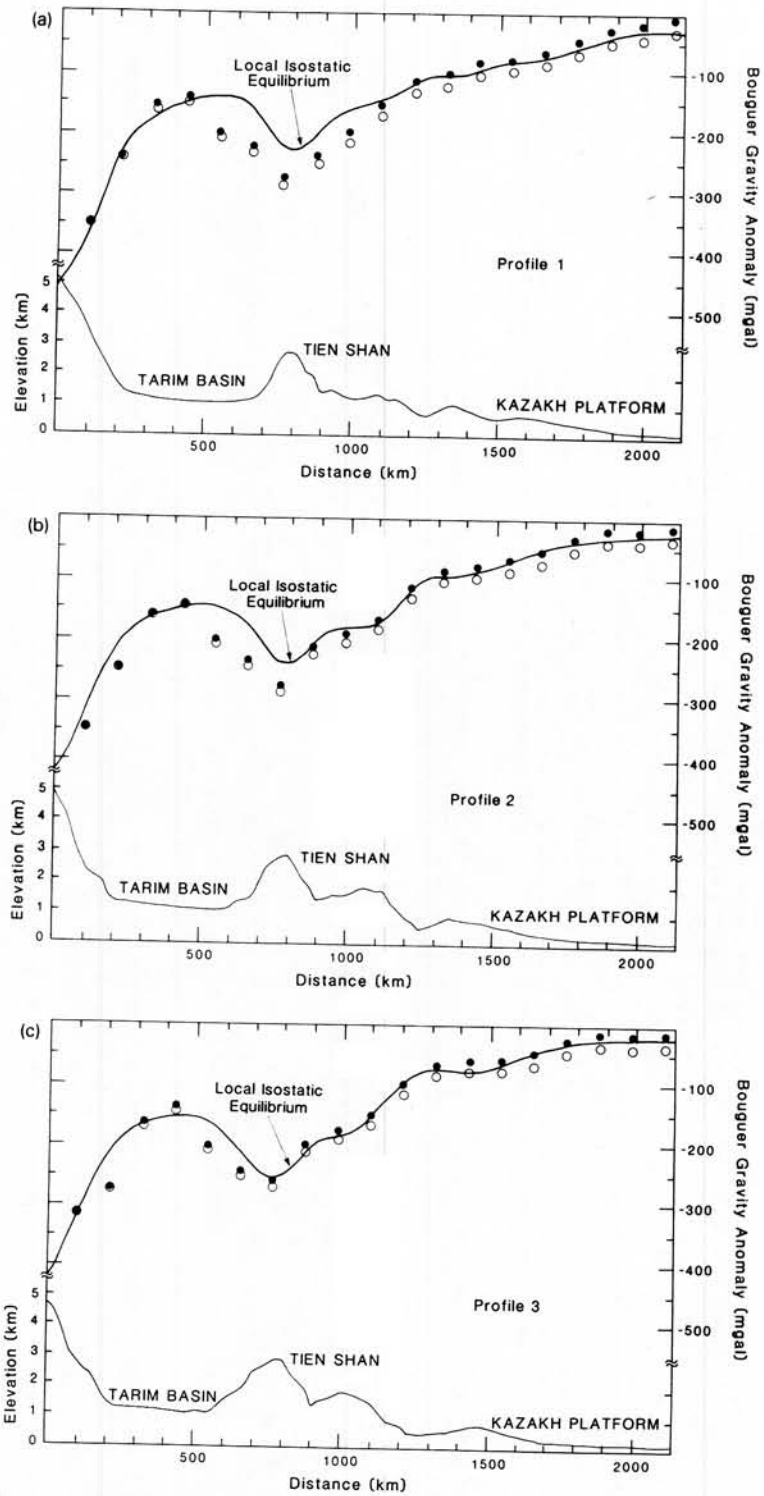


Fig. 2. Profiles of 1° ×1° complete Bouguer gravity anomalies, calculated Bouguer anomalies assuming local isostatic equilibrium, and elevations across the Tien Shan (see Fig. 1 for locations of profiles). Open circles show raw 1° ×1° average Bouguer gravity anomalies; closed circles show corresponding gravity anomalies with the contributions of the first 10 harmonics of the long-wavelength field [39] subtracted. These corrected data are used in all subsequent figures. The continuous line shows Bouguer gravity anomaly profiles that would be observed if the crust were in local Airy isostatic equilibrium. Note the significant deviations from isostatic equilibrium over the Tien Shan along profiles 1, 2, and 3, but not along profiles 4–6 or 8–10.

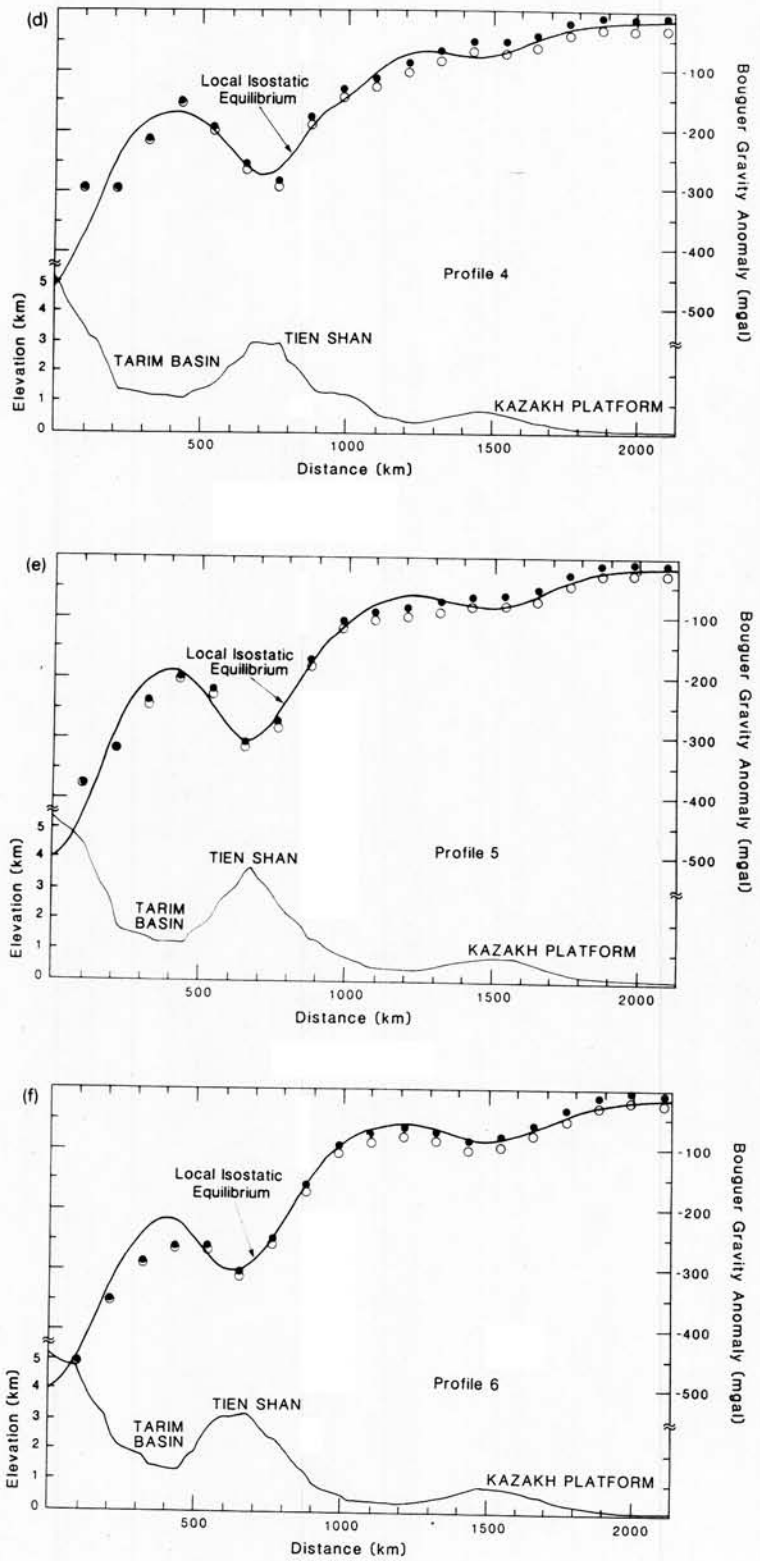


Fig. 2 (continued).

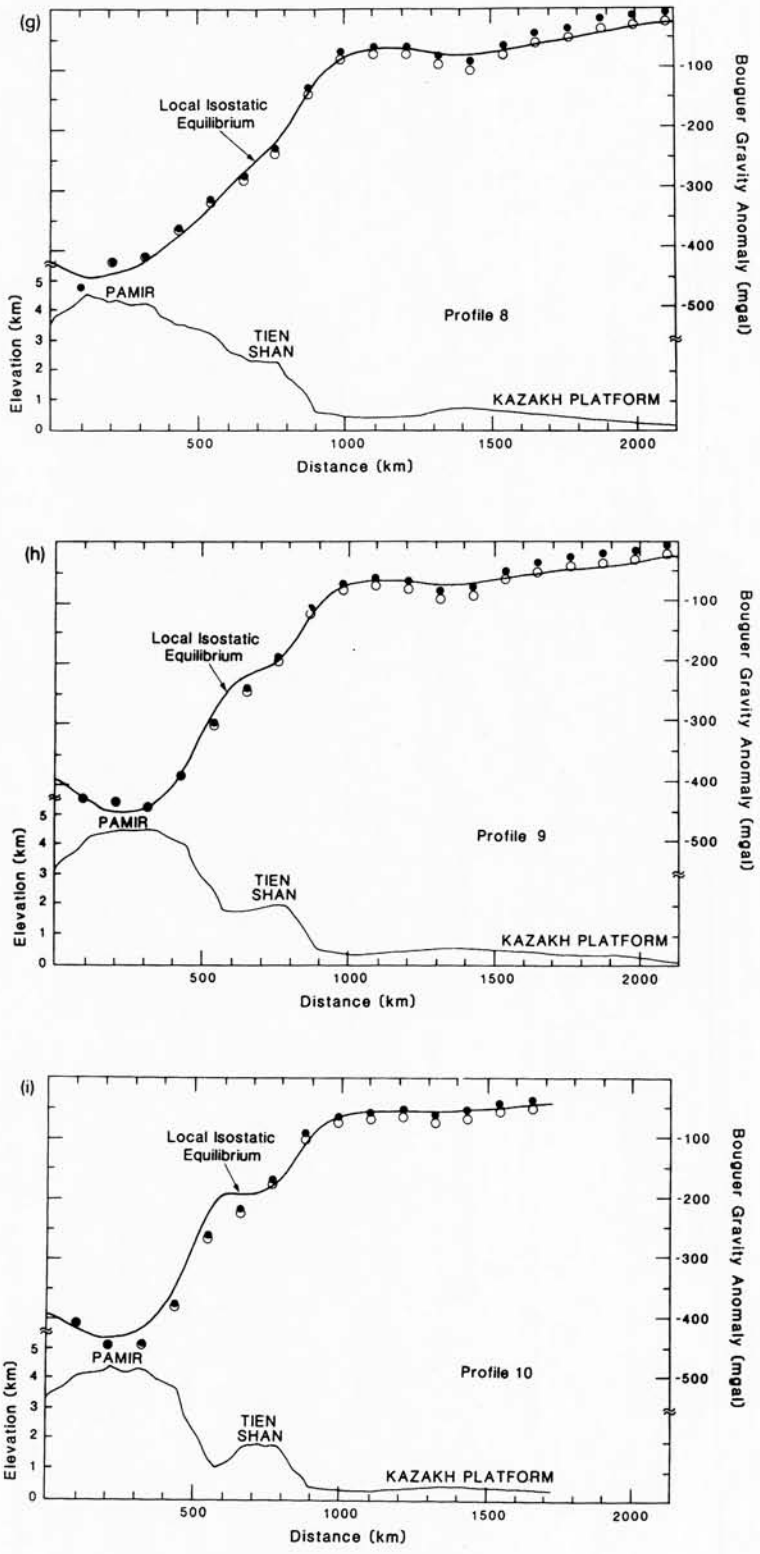


Fig. 2 (continued).

of each profile. We then smoothed the profiles by eye and resampled them at intervals of 111 km.

The long-wavelength gravity field includes a relatively steep northward gradient, decreasing by 20 mgal, across the region considered here. Accordingly, as shown in the profiles in Fig. 2, we subtracted the contribution from the first 10 harmonics of the Earth's gravity field GRIM3B-L1 [39] from these $1° \times 1°$ average values to obtain corrected average Bouguer anomalies, due primarily to density variations in the crust and upper mantle. Thus, our analysis considers only the gravity field with wavelengths shorter than about 4000 km.

*3.1. Deviations from local isostatic equilibrium*

Profiles of complete Bouguer gravity anomalies show the expected minima over the highest regions, the Tien Shan, the Pamir, and the northern edge of the Tibetan Plateau (Fig. 2), and the gross two-dimensional character of the relatively linear Tien Shan is reflected by the Bouguer anomalies. Our interest, however, is not so much in variations in crustal thickness, as in deviations from local isostatic equilibrium that might be manifestations of dynamic processes beneath the crust. To identify uncompensated mass anomalies, we calculated theoretical Bouguer anomalies assuming that the crustal thickness varies linearly with mean elevation according to Airy isostasy. We used an average crustal thickness of 50 km beneath the surrounding regions [34–36].

The region is nearly in local isostatic equilibrium; differences between calculated and observed anomalies are, in general, less than 10–20 mgal, particularly when the long-wavelength field is removed. For the three easternmost profiles, profiles 1, 2, and 3, however, large deviations from local isostatic equilibrium can be seen over the southern part of the Tien Shan and the northern margin of the Tarim Basin, where differences between calculated and observed anomalies exceed 50 mgal. The absence of such differences along profiles 4, 5, and 6 suggests that the portion of the Tien Shan transected by these profiles is essentially in local isostatic equilibrium. Similarly, the absence of large differences along profiles 8, 9, and 10 across the Pamir suggests that mass anomalies are small there also. This variation along the chain in deviations from local isostasy implies that the dynamic processes operating in the upper mantle also vary along the chain. Therefore, the cylindricity implied by the geologic history, by the present surface and crustal structure, and by the elevations of the chain may not obtain in the underlying mantle.

*3.2. Elastic plate model*

To analyze the gravity anomalies further, we used the simple model of an elastic plate overlying an inviscid fluid and loaded by the weight of the topography above it. The approach to solving the basic equation is given in Appendix A. Using the solutions for deflections of the plate to define polygonal blocks with densities of the sedimentary cover, the crust, and the mantle, we calculated gravity anomalies [40].

The fundamental parameter that governs the shape of the deflection is the flexural rigidity, $D$. For an elastic plate of thickness $T_E$:

$$D = E \cdot T_E^3/12(1 - \nu^2)$$

where $E$ is Young's modulus, and $\nu$ ($\approx 0.25$) is Poisson's constant. It is customary, much to the annoyance of one of us (P.M.), to express the flexural rigidity in terms of the thickness of an equivalent elastic plate, and therefore with the familiar dimension of kilometers, instead of, properly, in the less familiar Newton-meters. Here we give both, with equivalent thicknesses calculated assuming that $E = 8 \times 10^{10}$ N/m$^2$. For a value of $E$ more appropriate for the mantle ($1.6 \times 10^{11}$ N/m$^2$), equivalent elastic thicknesses would be 80% of those listed. Since these thicknesses have no physical meaning, a 20% difference is irrelevant.

Because we know the average elevations along the profiles, the only unknown parameter that characterizes the surface load is the density of the rock above sea level. Thus, the calculated deflection is dependent on only a small number of parameters. For a continuous plate, these parameters are the flexural rigidity and the difference in density between the sedimentary fill in the basins and the mantle. For a semi-infinite plate, we may also specify a force per unit length and a bending moment per unit length at the free end of the plate.

The elastic plate model is useful as a means for examining the support of mass anomalies, because

only one parameter, $D$, governs the effective strength of the plate. A plate with a large flexural rigidity can support essentially any mass anomaly, by distributing its load over a large area, but one with a small flexural rigidity only locally supports mass anomalies. In the limit of a very small flexural rigidity, Airy isostasy obtains.

*A note on densities.* In general, the calculated gravity field is insensitive to the density chosen for

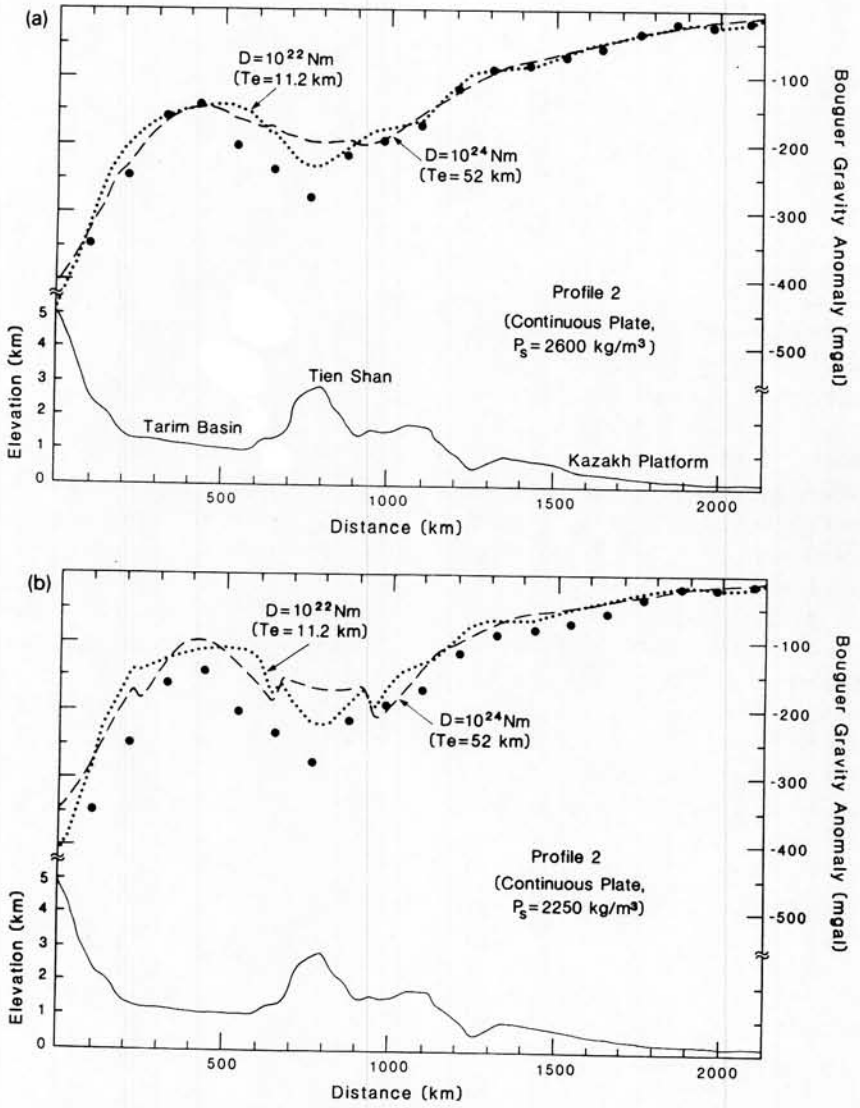


Fig. 3. Comparisons of corrected Bouguer gravity anomalies with those calculated for a continuous elastic plate flexed down by the weight of the topography above sea level, with different densities of material above the plate (e.g. sedimentary fill): (a) 2600 kg/m$^3$ and (b) 2250 kg/m$^3$. Neither a small flexural rigidity, $10^{22}$ N m ($T_E \approx 11.2$ km), nor a large value, $10^{24}$ N m ($T_E \approx 52$ km), works well. Consequently, in subsequent analyses we used two separate plates. Note also that with a density of the sedimentary fill in the basins of 2250 kg/m$^3$, the fit over the Tarim Basin is poor (b). Part of the poor fit results from the widely spaced data not sampling well the short wavelength gravity field, but note also that with this low density, the fit over the middle of the Tarim Basin also is poor. We used a density of 2600 kg/m$^3$ in subsequent analysis.

the material overlying the plate, such as sediment, in such a calculation for a flexed plate [12]. The calculated deflection of the plate is greater for a larger than for a smaller sediment density. Because the greater deflection is compensated by the smaller density difference between the mantle (with its density fixed at 3300 kg/m$^3$) and the sediment, the calculated gravity anomalies, however, are not seriously affected by using an erroneous density of the sedimentary fill. Exceptions occur where the plate is sharply flexed or where materials with different densities are juxtaposed near one another. With a small density of 2250 kg/m$^3$ of the sedimentary fill, sharp edge-effects are clear in calculated gravity anomalies near the margins of the basins, even for a continuous plate beneath the range (Fig. 3). With a spacing of data of roughly 100 km, however, these edge effects cannot be resolved by the data that we used.

Because both sides of the Tarim Basin are flexed down, the center of the basin is flexed up quite sharply. The amount of that flexure depends not only on the flexural rigidity, but also on the density difference between the sedimentary cover and upper mantle. Smaller densities of sediment, or greater density differences, yield larger deflections, as well as somewhat shorter characteristic wavelengths of the flexure. With low densities of sediment (2250–2400 kg/m$^3$) the calculated gravity anomalies over the center of the Tarim Basin are too large (Fig. 3), and we adopted a density of 2600 kg/m$^3$.

Although the density of 2600 kg/m$^3$ is high for sediment, especially unconsolidated sediment, it is not unreasonable for indurated sedimentary rock. The Tarim Basin is underlain by a sequence of well indurated Paleozoic sedimentary rock, and we suspect that part of the thick low density material in the basins flanking the Tien Shan consists of slices of this rock overthrust atop one another. Yudakhin [41] reported densities of sediment and Cenozoic sedimentary rock ranging from less than 2000 kg/m$^3$ to more than 2700 kg/m$^3$. Thus, the value of 2600 kg/m$^3$ clearly is plausible. Nevertheless, because this density is neither constrained well, nor laterally constant, we pay no attention to the calculated deflections of the plate.

*Continuous elastic plate.* With underthrusting of the lithosphere beneath both sides of the Tien Shan and crustal shortening throughout the range, a continuous plate is not likely to be a good model for the deep structure of the Tien Shan. Nevertheless, let us consider a continuous plate as an approximation to a strong upper mantle beneath the whole region. Using profile 2 as an example (Fig. 3), it is clear that only with a contrived set of mass anomalies within or beneath the plate could a continuous plate provide a useful fit to the observed data. A large deficit of mass over the southern part of the Tien Shan is required to match the large negative anomaly there, but only a very large flexural rigidity could allow that deficit to be localized without causing the calculated gravity field over the rest of the region to be too small. Only with a special set of forces on the base of such a plate could the gravity anomalies be matched. Allowing for different densities of the sedimentary fill in the basins adjacent to the plate does not improve the match (Fig. 3).

*Two separate converging plates.* Given underthrusting of both flanks of the range and distributed deformation across the range, a simple approximation is to consider two semi-infinite plates underlying the areas north and south of the range (Fig. 4). The breaks were chosen to lie at the minima in the Bouguer anomaly profiles. For the purposes of the calculations, we can treat the two plates independently, with different flexural rigidities and with appropriate, separate loads on each. Moreover, at the free ends, beneath the Tien Shan, we can assign bending moments and forces per unit length to each plate separately. We use such a simple model to constrain the flexural rigidities of the plates and the forces that must be applied to each in order to match the gravity data, but we do not imagine that two separate elastic plates are rammed against one another beneath the axis of the Tien Shan. We use this simple model merely to quantify the parameters that govern the deviations from local isostatic equilibrium, not to simulate the dynamic processes occurring beneath the range.

First, we searched for acceptable, and then better, matches of calculated and observed Bouguer anomaly profiles by varying the flexural rigidities and the forces and moments per unit length at the ends of the plates. Values of $D > 10^{25}$ N m ($T_E > 110$ km) yield calculated gravity anomaly profiles that are too smooth to match

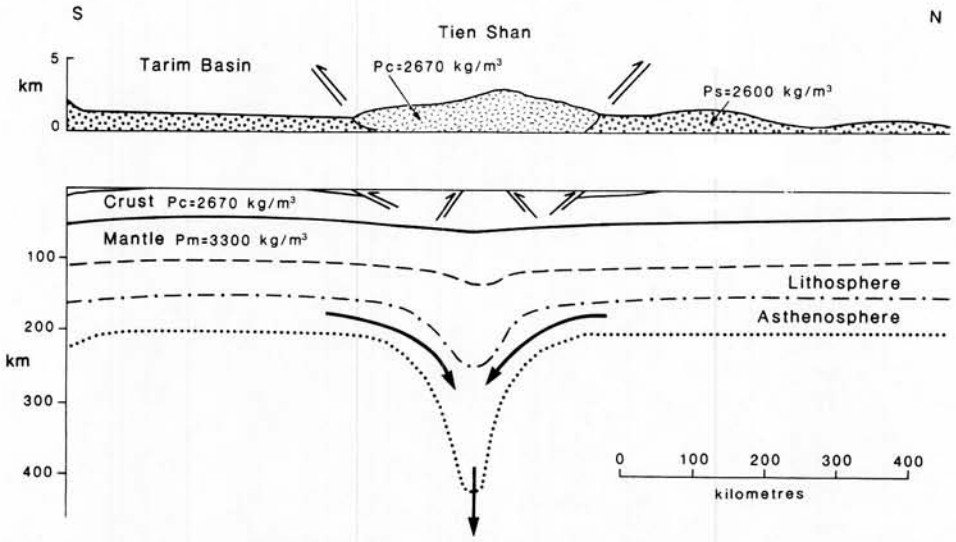


Fig. 4. Sketch of the simple image that we have of the deep structure of the Tien Shan. Lithosphere underthrusts the range from both sides and is flexed down by the weight of the mountain range. The shortening occurring within the range must be associated with similar horizontal shortening in the underlying mantle. Consequently, the weight of the thickened mantle lithosphere might flex the plates down more than that due to the load imposed by the weight of the mountains. Moreover, the thickened lithospheric root might detach, sink into the asthenosphere, and drive a circulation that imposes dynamic stresses to the base of the remaining lithosphere above and pulls it down. This sketch illustrates the basic, simple *qualitative* image that we have of the deep structure of the eastern Tien Shan.

those observed; wavelengths are too long (Fig. 5). It is readily apparent that the flexural rigidities of the two plates are very different. For the northern side, a plate with $D \approx 10^{24}$ N m ($T_E \approx 50$–$60$ km) yields a poor fit; calculated gravity anomaly profiles do not show the clear variations that correlate with variations in topography over distances of 200–300 km (Fig. 5). The flexural rigidity must be less than $10^{23}$ N m ($T_E < 25$ km). For flexural rigidities of $10^{23}$ N m, calculated gradients on the south side are too steep, and a value near $10^{24}$ N m ($T_E \approx 50$–$60$ km) seems to be required (Fig. 5). This value is similar to that inferred for the south side of the Tarim Basin [42].

For profiles 4–6 and 8–10, local isostatic equilibrium yields an adequate match to observed average anomalies, and no additional forces or moments need to be applied to the ends of the plate (Fig. 2). For profiles 1, 2, and 3, acceptable fits could not be obtained without specifying such a force per unit length or bending moment per unit length to the end of the southern plate. The value of the force or moment per unit length needed to yield an acceptable fit to the observed data depends on the value of $D$ (Fig. 5), with larger forces or moments for larger flexural rigidities (see also [12]).

To evaluate the maximum sizes of likely forces per unit length or bending moments per unit length, we carried out a series of tests with different flexural rigidities for each of profiles 1, 2, and 3. For each, we assumed no bending moment and compared calculated gravity anomalies obtained with a variety of forces, and then set the force to zero and did the same with different bending moments. Here, we show only the results with one flexural rigidity for each of the plates and with a small moment per unit length of $2 \times 10^{16}$ N applied to the ends of the plates.

For the north side, the calculations shown use forces and moments, but both are small. Although the matches to the data for profiles 2–6 are better with such small forces and moments, their magnitudes are not well resolved (Figs. 2, 5, and 6). Profile 1 cannot be matched without a force per unit length, but even with one, the fit is not very good. In any case, although a more complex physical model may be required, the small number of data does not make adding complexities useful at present.

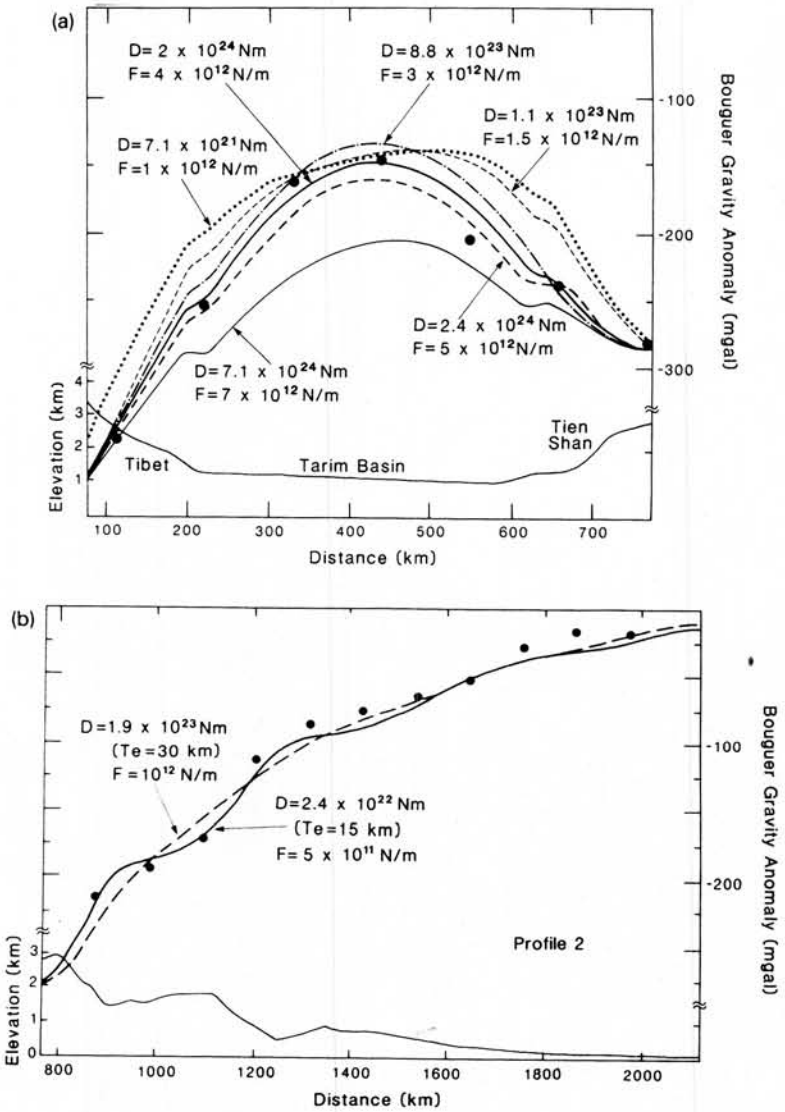


Fig. 5. Comparisons of corrected Bouguer gravity anomalies along profile 2 with those calculated for plates with different flexural rigidities and different forces per unit length applied to the ends of them. A flexural rigidity of $D \approx 10^{24}$ N m ($T_E \approx 50$–$60$ km) is required for the southern plate (a), but a value of $D < 10^{23}$ N m ($T_E < 25$ km) is required for the northern plate (b). These plots were constructed by fixing the flexural rigidity and searching for a force that yielded the best (or least bad) fit. Thus, for a given value of $D$, other forces per unit length will not improve the fits. In all cases, a bending moment per unit length of $2 \times 10^{16}$ N is applied. For most flexural rigidities ($D > 10^{23}$ N m), this small moment has no effect, but for very small flexural rigidities it does improve the fit.

For the south side, the large differences between observed and calculated gravity anomalies along profiles 1, 2, and 3 require that forces per unit length pull the plates down (Figs. 5 and 6). For $D = 1.5 \times 10^{24}$ N m, the force needed to deflect the southern plate sufficiently is $4 \times 10^{12}$ N/m, roughly comparable with that used for the Himalaya [12,13]. If the flexural rigidity of the southern plate were the same along the range, the magnitude of such an inferred downward force would decrease westward to essentially zero for profiles 1, 2, and 3. Because of the dependence of the inferred force on the assumed flexural rigidity, and because a bending moment, instead of a force, can also contribute to the deflection of the plate, it is unwise to attribute much significance to the

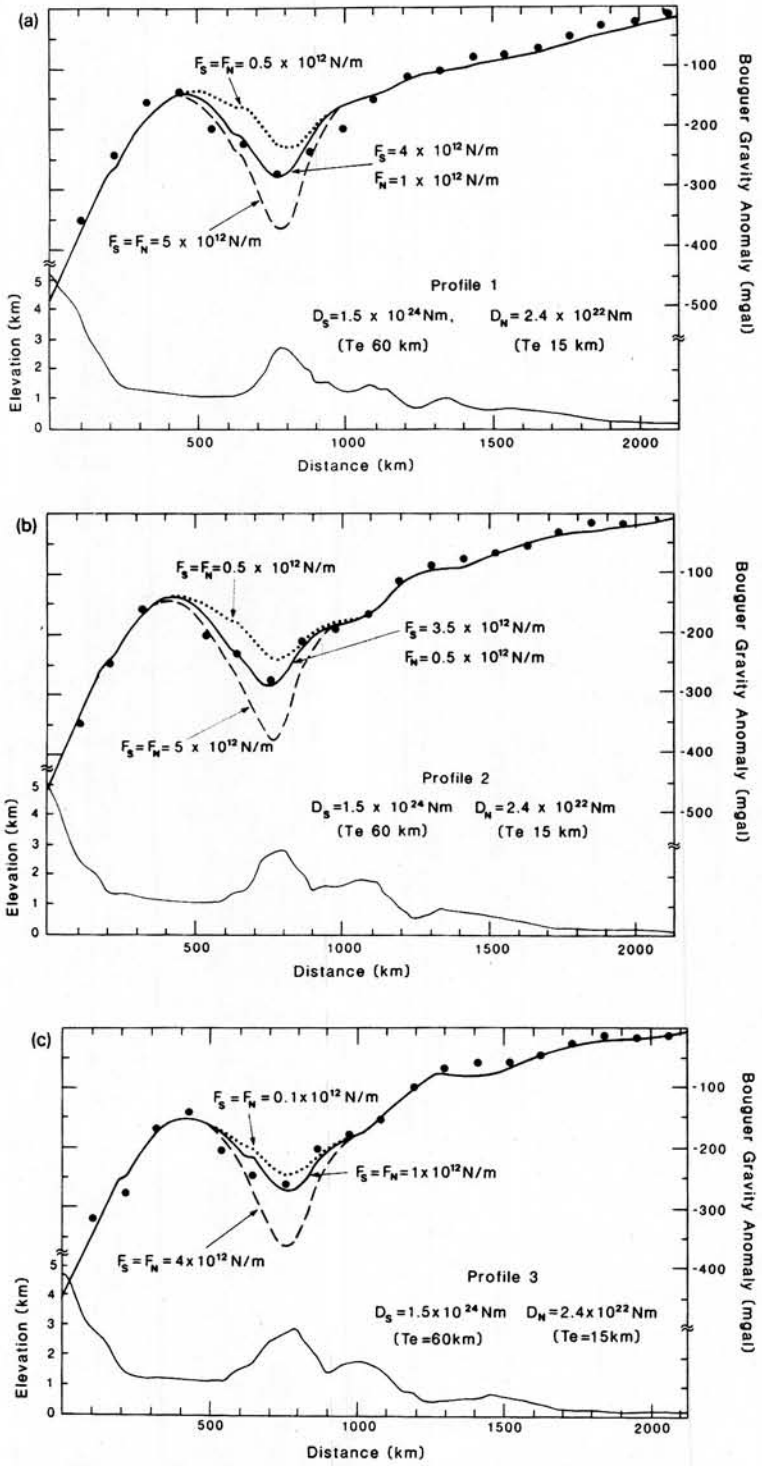


Fig. 6. Comparisons of corrected Bouguer gravity anomalies along profiles 1, 2, and 3, with those calculated for different forces per unit length applied to the ends of the southern and northern plates. Note that a larger force is needed for profile 1 than for profiles 2 and 3. In all cases shown, $D = 1.53 \times 10^{24}$ N m ($T_E \approx 60$ km) for the southern plate, and $D = 2.4 \times 10^{22}$ N m ($T_E \approx 15$ km) for the northern plate, and a bending moment per unit length of $2 \times 10^{16}$ N is applied to each plate. For larger assumed values of $D$, larger forces per unit length would be needed, but the differences in such forces would be less than the differences between those needed for neighboring profiles. Profiles could also be matched adequately with small forces and with large bending moments, but the magnitude of the required bending moment would similarly increase eastward.

magnitudes of the forces per unit length, except to note that the values are reasonable.

Finally, we also note that we made calculations with a laterally varying flexural rigidity. The additional flexibility in the calculations allowed fits with relatively small values of $D$ beneath the Tien Shan and somewhat larger values of $D$ beneath the Tarim Basin than those shown here. Inclusion of a variable flexural rigidity, however, did not alter the basic conclusions that the flexural rigidity north of the chain must be less than that south of it and that additional forces must be applied to the southern plate along profiles 1, 2, and 3.

## 4. Implications for dynamic processes

The analysis of gravity anomalies described above implies that some process has caused the crust of the eastern part of the Tien Shan to be out of local isostatic equilibrium, but that whatever the process is, it does not act along the whole of the chain. That analysis also shows that the deviations from local isostatic equilibrium cannot be due to the strength of the lithosphere supporting mass deficits, or mass excesses, in the crust. Some deeper process must cause the departure from local isostasy.

One can imagine two simple mechanisms that can cause deviations from local isostatic equilibrium: the force exerted by gravity acting on a deep mass attached to the plate could pull it down, or dynamic stresses associated with convective flow in the asthenosphere could also do so.

A deep anomalous mass will generate gravity anomalies that we have not yet considered. If such a mass were sufficiently deep, its contribution to the gravity field would be a low-amplitude, long-wavelength signal, which might not be detectable with the sparse data that we have. The contribution to gravity anomalies by a localized mass per unit length, $M$, at a depth, $z_0$, and with horizontal coordinate $x = 0$ is given by:

$$\Delta g = 2 \cdot M \cdot G \cdot z_0 / \left(x^2 + z_0^2\right)$$

where $G$ is Newton's gravitational constant. A force per unit length of $1\text{–}4 \times 10^{12}$ N/m, if due to a two-dimensional mass anomaly at depth, would imply a mass per unit length of $1\text{–}4 \times 10^{11}$ kg/m. If centered at a depth of 100 km, then its maximum contribution to the gravity field would be 13–50 mgal, decaying to 6–25 mgal at a distance of 100 km. If it were centered at a depth of 200 km, the maximum anomaly would be half as great (6–25 mgal), and the average gradient would be four times smaller. We think that a mass per unit length of $4 \times 10^{11}$ kg/m at a depth of 100 km should be detectable, but the same mass at greater depth, or a smaller mass at roughly 100 km, could be hidden in the sparse gravity data that we use. Thus, we think that gravity acting on such a static deep mass could provide the additional force per unit length deflecting the plate.

Convective circulation in the asthenosphere exerts dynamic stresses on the lithosphere. Regions of upwelling generally are associated with dynamically supported positive topography and positive gravity anomalies, relative to isostatic equilibrium, and regions of downwelling are associated with depressions and negative gravity anomalies [43–46]. In all such calculations, the stress that deflects the topography is proportional to the viscosity of the material, which is not well enough constrained to make a calculation of predicted topography more than very approximate. Nevertheless, let us consider an idealized case for which an analytic solution can be given.

In Appendix B, we derive expressions for the normal stress at the base of a plate that undergoes lateral compression and that overlies an incompressible fluid moving laterally beneath the plate toward a corner and then downward. We assume further that the fluid undergoes horizontal compression (and vertical extension) as it moves laterally toward the corner and vertical extension (and horizontal compression) as it moves downward. This is clearly a severe idealization, and we use it merely to illustrate plausible stresses and deflections for plausible strains, velocities, and viscosities.

The deviatoric normal stress $\sigma$ applied to the base of the overlying plate by such flow is given by $\sigma = 2\eta\epsilon$, where $\epsilon$ is the strain rate (tensional deviatoric stresses and strains are positive) and $\eta$ is viscosity (Appendix B). The deviations from isostatic equilibrium on profiles 1, 2, and 3 suggest deficits of mass equivalent to excess crustal thicknesses of up to 6 km, for a density contrast at the Moho of 500 kg/m$^3$. Such deflections could be maintained by a tensional deviatoric stress of 30 MPa applied to the base of the crust, or litho-

sphere. If that stress were maintained dynamically by flow beneath a region undergoing horizontal compressive strain at $3 \times 10^{-15}$/s (10 mm/a over a width of 100 km), it would require a viscosity of roughly $5 \times 10^{21}$ Pa s. Such a viscosity is large for the asthenosphere, but probably not too large for an average for the thermal boundary layer at the base of the lithosphere. Thus we think that dynamic stresses arising from convergent flow and downwelling beneath the range could account for the deviations from isostatic equilibrium.

## 5. Conclusions

Average Bouguer gravity anomalies on profiles across the Tien Shan show the characteristic negative anomalies over the areas of high elevations and suggest that local isostatic compensation is nearly complete. Deviations from isostatic compensation, however, do exist for the profiles across the eastern part of the range and show a deficit in mass there.

Comparisons of measured and calculated gravity anomalies for elastic plates loaded by the weight of the mountain range show that the flexural rigidity of the plate beneath the area north of the Tien Shan must be less than about $10^{23}$ N m ($T_E < 25$ km), but that for the area south of the range, beneath the Tarim Basin, it must be larger, $D \approx 10^{24}$ N m ($T_E \approx 50$–$60$ km). Gravity anomalies over the eastern part of the Tien Shan require the existence of an additional force to deflect the plate extending beneath the southern part of the range. The weight of the mountain range is inadequate to flex that plate down enough to cause the large Bouguer gravity anomalies observed over the range and over the basin south of it.

The force per unit length causing deviations from isostatic equilibrium could be due to the static force of gravity acting on cold material (a thickened lithospheric root) beneath the range or to dynamically induced viscous stresses arising from convergent flow and downwelling beneath the range. Neither the gravity data, nor the parameters that describe such processes, however, are known well enough to allow either process to be ruled out, or to constrain the relative contributions of each in combination with one another. Clearly a combination of them is likely.

What may ultimately be most important is that the deviations from isostatic equilibrium vary markedly *along the chain*. Therefore, whatever dynamic processes are responsible for such deviations must also vary along the chain. Hence the apparently similar geologic history along the Tien Shan seems to conceal an important variation in the deep structure and mantle dynamics along it. Lateral variation in upper mantle structure along the Tien Shan is also indicated by the distribution of teleseismic P-wave residuals at seismograph stations in the Tien Shan [36,37,48]. Unfortunately the area where gravity anomalies are most suggestive of cold material in the upper mantle lies outside the region studied by Vinnik, Saipbekova, and Yudakhin [36,47,48].

Suppose the large negative Bouguer gravity anomalies beneath the eastern Tien Shan, which reflect a deficit of mass there, were due to thickening of the lithosphere and to downwelling of material beneath the range. Suppose also that such a process either did not occur or were no longer occurring beneath the western part of the Tien Shan. Then, the downward flow beneath the eastern Tien Shan might draw mantle material from the western Tien Shan into the downward plume. This is the pattern of convection expected from two-dimensional numerical experiments [9], and it suggests that the detachment and sinking of a cold lithospheric root would not necessarily be the same in all cross sections across the chain. Instead, variations in the deep structure *along* such chains might be at least as great as, if not greater than, those across them.

## Acknowledgements

We thank M. Diament, M.K. McNutt, and B. Parsons for help and advice on aspects of this work. Diament and two anonymous reviewers offered constructive criticism of the manuscript. This work was supported in part by the cooperative program between the Academy of Sciences of the USSR and the Centre National de la Recherche Scientifique in France, by the National Science Foundation in the U.S. through grant EAR-8817220 and by National Environmental Research Council in the U.K. through grant GR3/7032. P.M. also thanks Royal Society for a Visiting Research Fellowship.

## Appendix A—Method for solving the basic equation governing flexure

If an elastic plate overlies an inviscid fluid, and if loads on it vary only in one horizontal direction, then the deflection, $w(x)$, is given by:

$$\frac{d^2}{dx^2}\left[D(x)\frac{d^2w(x)}{dx^2}\right] + \frac{d}{dx}\left[F_H(x)\frac{dw(x)}{dx}\right] + [\rho_M - \rho_S]\cdot g\cdot w(x) = F_V(x) \quad \text{(A1)}$$

where $D(x)$, the flexural rigidity, is defined in the text, $F_H(x)$ and $F_V(x)$ are horizontal and vertical forces per unit length, $\rho_M$ and $\rho_S$ are densities of the underlying mantle and overlying material (sediment or crust), and $g$ is gravity.

In all cases we assumed that $F_H = 0$. As $x$ approaches $\infty$, $w(x)$ and $dw(x)/dx$ approach zero. Integrating (A1) over $x$, and recognizing that because of isostasy, the integral of the third term on the left must equal the integral of the right side, we have another boundary condition:

$$\frac{d}{dx}\left[D(x)\frac{d^2w(x)}{dx^2}\right] = 0, \text{ at } x = 0$$

Note that the bending moment is given by $M(x) = -D(x)\cdot d^2w(x)/dx^2$.

Following Sheffels and McNutt [15], using procedures defined by Dahlquist and Bjorck [49], we solved (A1) numerically using a finite difference technique. We considered a plate that extends a distance of 5–6 flexural parameters beyond the region of interest. We compared calculated deflections made with spacings of $x$ between 5 and 50 km, and found differences of less than 1% for this range. Accuracies diminished for $x > 50$ km, and we used a sampling at intervals of 25 km. We tested the routine by comparing the numerical results with the analytic solution for a plate loaded at the end and found differences of less than 1% for all points, except at the few points near the ends of the plate, where we have no data.

## Appendix B—Simple analysis of the flow of a fluid undergoing horizontal compression as it approaches a corner

Consider a quarter space in which incompressible flow occurs with velocities, $v(x, z)$ or $v(r, \theta)$ toward the corner along one side and away from it on the other. The speed along the boundaries is proportional to a constant strain rate and to the distance from the corner:

$$v_x(x, 0) = -\epsilon\cdot x$$
$$v_z(0, z) = \epsilon\cdot z$$
$$v_z(x, 0) = 0$$
$$v_x(0, z) = 0$$

where $\epsilon$ is a positive strain rate, and extension is positive. The horizontal velocity at the surface ($z = 0$) is toward the corner, and the vertical velocity below the corner ($x = 0$) is downward (positive $z$). The velocity vanishes at the corner.

Using a stream function and cylindrical coordinates to describe the velocity field:

$$v_r = (1/r)\cdot \partial\psi/\partial\theta$$
$$v_\theta = -\partial\psi/\partial r$$

The basic equation governing the flow in the fluid is the biharmonic equation, and if we let $\psi = r^2\cdot f(\theta)$ [50], that equation reduces to:

$$(1/r^2)\cdot[f^{iv}(\theta) + f''(\theta)] = 0$$

for which the solution is:

$$\psi(r, \theta) = r^2\cdot[a\sin 2\theta + b\cos 2\theta + c\,\theta + d]$$

In cylindrical coordinates, the boundary conditions are:

$$v_r = -\epsilon\cdot r \text{ and } v_\theta = 0 \quad \text{at } \theta = 0$$
$$v_r = \epsilon\cdot r \text{ and } v_\theta = 0 \quad \text{at } \theta = \pi/2$$

from which we obtain $b = c = d = 0$, and $a = -\epsilon/2$: $\psi = -(\epsilon\cdot r^2/2)\sin 2\theta$.

The stresses are given by $\sigma_{ij} = -P\cdot\delta_{ij} + 2\cdot\eta\cdot\epsilon_{ij}$, where $\sigma_{ij}$ and $\epsilon_{ij}$ are the stress and strain tensors, $P$ is the dynamic pressure, $\eta$ is viscosity, and $\delta_{ij}$ is the Kronecker delta function. Using the Navier-Stokes equation to evaluate the pressure, we find that it is a constant, independent of $r$ and $\theta$. Thus, we can set it to zero, and $\sigma_{rr} = 2\cdot\eta\cdot\epsilon_{rr}$, and $\sigma_{\theta\theta} = 2\cdot\eta\cdot\epsilon_{\theta\theta}$. Hence, $\sigma_{rr} = -2\cdot\eta\cdot\cos 2\theta$, $\sigma_{\theta\theta} = 2\cdot\eta\cdot\cos 2\theta$, $\sigma_{r\theta} = 2\cdot\eta\cdot\sin 2\theta$, and, most importantly, $\sigma_{\theta\theta}$ is a positive, and therefore tensile, deviatoric stress at $\theta = 0$. Hence, the surface below the zone of crustal shortening should be pulled down.

Suppose $\epsilon = (10 \text{ mm/a})/(100 \text{ km}) = 3\times 10^{-15}$/s. For $\eta = 5\times 10^{20}$, $5\times 10^{21}$, or $5\times 10^{22}$ Pa s, $\sigma = 3$ MPa, 30 MPa, or 300 MPa.

## References


1 I.V. Mushketov, Materials for the study of earthquakes of Russia, 62 pp., A.S. Suvorin, St. Petersburg, 1891 (in Russian).

2 N.V. Kondorskaya and N.V. Shebalin, eds., New Catalog of Strong Earthquakes in the Territory of the USSR, 535 pp., Nauka, Moscow, 1977 (in Russian).

3 Deng Qidong, Xu G., Fan F. and Zhang Y., The Seismotectonic Map of the People's Republic of China, Cartographic Publishing House, Beijing, 1979.

4 P. Molnar and Deng Qidong, Faulting associated with large earthquakes and the average rate of deformation in central and eastern Asia, J. Geophys. Res. 89, 6203–6227, 1984.

5 Feng Xianyue, Paleoseismological study of the Kaxhe fault zone, Xinjiang, Seismol. Geol. 9, 74–77, 1987 (in Chinese).

6 P. Molnar and W.-P. Chen, Seismicity and mountain building, in: Mountain Building Processes, K. Hsü, ed., pp. 41–57, Academic Press, London, 1982.

7 P. Molnar and H. Lyon-Caen, Some simple physical aspects of the support, structure, and evolution of mountain belts, in: Processes in Continental Lithospheric Deformation, Geol. Soc. Am. Spec. Pap. 218, 179–207, 1988.

8 M.R. Nelson, R. McCaffrey and P. Molnar, Source parameters for 11 earthquakes in the Tien Shan, Central Asia, determined by P and SH waveform inversion, J. Geophys. Res. 92, 12629–12648, 1987.

9 G.A. Houseman, D.P. McKenzie and P. Molnar, Convective instability of a thickened boundary layer and its relevance for the thermal evolution of continental convergent belts, J. Geophys. Res., 86, 6115–6132, 1981.

10 L. Fleitout and C. Froidevaux, Tectonics and topography for a lithosphere containing density heterogeneities, Tectonics 1, 21–56, 1982.

11 G.F. Panza and St. Müller, The plate boundary between Eurasia and Africa in the Alpine area, Mem. Sci. Geol. 33, 43–50, 1979.

12 H. Lyon-Caen and P. Molnar, Constraints on the structure of the Himalaya from an analysis of gravity anomalies and a flexural model of the lithosphere, J. Geophys. Res. 88, 8171–8191, 1983.

13 H. Lyon-Caen and P. Molnar, Gravity anomalies, flexure of the Indian plate, and the structure, support and evolution of the Himalaya and Ganga Basin, Tectonics 4, 513–538, 1985.

14 E. Humphreys, R.W. Clayton and B.H. Hager, A tomographic image of mantle structure beneath southern California, Geophys. Res. Lett. 11, 625–627, 1984.

15 B. Sheffels and M. McNutt, Role of subsurface loads and regional compensation in the isostatic balance of the Transverse Ranges, California: Evidence for intracontinental subduction, J. Geophys. Res. 91, 6419–6431, 1986.

16 E. Norin, Geology of the Quruq Tagh, Eastern Tien Shan, Reports from the Scientific Expedition to the Northwestern Provinces of China under the Leadership of Dr. Sven Hedin, III. Geology, 1, 194 pp., Bokforlags Aktiebolaget Thule, Stockholm, 1937.

17 E. Norin, Geologic Reconnaissance in the Chinese Tien Shan, Reports from the Scientific Expedition to the Northwestern Provinces of China under the Leadership of Dr. Sven Hedin, III. Geology, 6, 229 pp., Tryckeri Aktiebolaget Thule, Stockholm, 1941.

18 V.S. Burtman, Structural geology of the Variscan Tien Shan, USSR, Am. J. Sci. 272A, 157–186, 1975.

19 A.M. Babaev, G.V. Koshlakov and K.M. Mirzoev, Seismic Regionalization of Tadjikistan, 67 pp., Donish, Dushanbe, 1978 (in Russian).

20 Zh.M. Zhang, J.G. Liou and R.G. Coleman, An outline of the plate tectonics of China, Geol. Soc. Am. Bull. 95, 295–312, 1984.

21 C.F. Burrett, Plate tectonics and the fusion of Asia, Earth Planet. Sci. Lett. 21, 181–189, 1974.

22 A.M.C. Şengör, D. Altiner, A. Cin, T. Ustaömer and K.J. Hsü, Origin and assembly of the Tethyside orogenic collage at the expense of Gondwana Land, in: Gondwana and Tethys, M.G. Audley-Charles and A. Hallam, eds., Geol. Soc. London, Spec. Publ. 37, 119–181, 1988.

23 B.F. Windley, M.B. Allen, C. Zhang, Z.-y. Zhao and G.-r. Wang, Paleozoic accretion and Cenozoic redeformation of the Chinese Tien Shan Range, Central Asia, Geology, in press, 1989.

24 V.N. Krestnikov, History of the development of oscillating movements of the Earth's crust of the Pamir and adjacent parts of Asia, 175 pp., Acad. Nauk, Moscow, 1962 (in Russian).

25 K.I. Bogdanovitch, I.M. Kark, B.Ya. Korolkov and D.I. Mushketov, The Earthquake in the Northern Districts of the Tien Shan, 22 December 1910 (4 January 1911) Commission of the Geology Committee, St. Petersburg, 1914 (in Russian).

26 A.V. Goryachev, Mesozoic-Cenozoic structure, history of tectonic development, and seismicity of the region of the lake Issyk-Kul, 179 pp., Acad. Nauk, Moscow, 1959 (in Russian).

27 V.I. Makarov, New tectonic structures of the Central Tien Shan, Trans. Vol. 307, 171 pp., Order of the Red Banner Geology Institute, Acad. Sci., Moscow, 1977 (in Russian).

28 A.A. Nikonov, A.V. Vavko and I.A. Veselov, Seismotectonics and Earthquake in the Zone of Convergence of the Pamir and Tien Shan, 240 pp., Nauka, Moscow, 1983.

29 V.I. Knauf and E.V. Khristov, Basic features of the tectonics of the Tien Shan, in: The Lithosphere of the Tien Shan, I.Ye. Gubin, ed., pp. 4–13, Nauka, Moscow, 1986.

30 E.I. Shirokova, General regularities in the orientation of principal stresses in the foci of earthquakes of the Mediterranean-Asiatic seismic belt, Izv. Acad. Sci. USSR, Phys. Solid Earth 1, 23–36, 1967 (in Russian).

31 E.I. Shirokova, Detailed study of the stresses and fault planes at earthquake foci of Central Asia (in Russian), Izv. Acad. Sci. USSR, Phys. Solid Earth 11, 22–36, 1974.

32 J. Ni, Contemporary tectonics in the Tien Shan region, Earth Planet. Sci. Lett. 41, 347–355, 1978.

33 P. Tapponnier and P. Molnar, Active faulting and Cenozoic tectonics of the Tien Shan, Mongolia and Baykal Regions, J. Geophys. Res. 84, 3425–3459, 1979.

34 V.I. Ulomov, Dynamics of the Earth's Crust and Prediction of Earthquakes, 214 pp., Fan, Tashkent, 1974 (in Russian).

35 I.S. Volvovsky and B.S. Volvovsky, Cross sections of the Earth's crust of the territory of the USSR from data of deep seismic sounding, 268 pp., Soviet Radio, Moscow,

1975. (English translation: Addis Translations International, Portola Valley, Calif., 1978).
36 L.P. Vinnik, A.M. Saipbekova and F.N. Yudakhin, Deep structure and dynamics of the lithosphere of the Tien Shan, in: The Lithosphere of the Tien Shan, I.Ye. Gubin, ed., pp. 143–146, Nauka, Moscow, 1986.
37 P. Molnar and P. Tapponnier, Cenozoic tectonics of Asia: effects of a continental collision, Science 189, 419–426, 1975.
38 M.J. Terman, C.C. Woo, D.C. Alverson, D.P. Cox and A.J. Woloshin, Atlas of Asia and Eastern Europe—to support detection of underground nuclear explosions, Vol. 2, Tectonics, U.S. Geological Survey, Reston, Va., 1967.
39 C. Reigber, G. Balmino, H. Müller, W. Bosch and B. Moynot, GRIM gravity model improvement using LAGEOS (GRIM3-L1), J. Geophys. Res. 90, 7285–7299, 1985.
40 M. Talwani, J.L. Worzel and M. Landisman, Rapid gravity computation for two dimensional bodies with application to the Mendocino submarine fracture zone, J. Geophys. Res. 64, 49–59, 1959.
41 F.N. Yudakhin, Density, in: The Lithosphere of the Tien Shan, I.Ye. Gubin, ed., pp. 31–33, Nauka, Moscow, 1986.
42 H. Lyon-Caen and P. Molnar, Gravity anomalies and the structure of western Tibet and the southern Tarim Basin, Geophys. Res. Lett. 11, 1251–1254, 1984.
43 D. McKenzie, Surface deformation, gravity anomalies and convection, Geophys. J. R. Astron. Soc. 48, 211–238, 1977.
44 B. Parsons and S. Daly, The relationship between surface topography, gravity anomalies, and temperature structure of convection, J. Geophys. Res. 88, 1129–1144, 1983.
45 M.A. Richards and B.H. Hager, Geoid anomalies in a dynamic mantle, J. Geophys. Res. 89, 5987–6002, 1984.
46 Jian Lin and E.M. Parmentier, Surface topography due to convection in a variable viscosity fluid: Application to short wavelength gravity anomalies in the central Pacific Ocean, Geophys. Res. Lett. 12, 357–360, 1985.
47 L.P. Vinnik and A.M. Saipbekova, Structure of the lithosphere and asthenosphere of the Tien Shan, Ann. Geophys. 2, 621–626, 1984.
48 F.N. Yudakhin, Toward the question of the dynamics of the lithosphere of the Tien Shan to the whole complex of geophysical data, in: The Lithosphere of the Tien Shan, I.Ye. Gubin, ed., pp. 31–33, Nauka, Moscow, 1986.
49 G. Dahlquist and A. Bjorck, Numerical Methods, 573 pp., Prentice Hall, Englewood Cliffs, N.J., 1974.
50 G.K. Batchelor, An Introduction to Fluid Mechanics, 615 pp., Cambridge University Press, Cambridge, 1967.